Comparison of the Base Excision and Direct Reversal Repair Pathways for Correcting 1,N^6-Ethenoadenine in Strongly Positioned Nucleosome Core Particles

Paul J. Caffrey†, Raadhika Kher†, Ke Bian‡,Δ, Deyu Li‡, Sarah Delaney,†*

†Department of Chemistry, Brown University, Providence, RI 02912

‡Department of Biomedical and Pharmaceutical Sciences, College of Pharmacy, University of Rhode Island, Kingston, RI 02881

ΔCurrent address: Department of Biology, Massachusetts Institute of Technology, Cambridge, MA 02139

Table of Contents Graphic

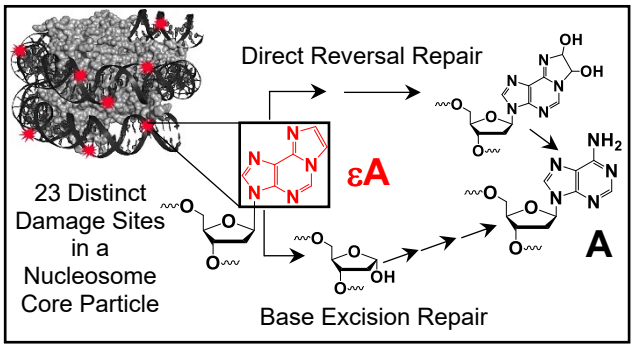

ABSTRACT

1,N^6-ethenoadenine (εA) is a mutagenic lesion and biomarker observed in numerous cancerous tissues. Two pathways are responsible for its repair: base excision repair (BER) and direct reversal repair (DRR). Alkyladenine DNA glycosylase (AAG) is the primary enzyme that excises εA in BER, generating stable intermediates that are processed by downstream enzymes. For DRR, the Fe(II)/α-ketoglutarate-dependent ALKBH2 enzyme repairs εA by direct conversion of εA to A. While the molecular mechanism of each enzyme is well understood on unpackaged duplex DNA, less is known about their actions on packaged DNA. The nucleosome core particle (NCP) forms the minimal packaging unit of DNA in eukaryotic organisms and is comprised of 145-147 base pairs wrapped around a core of eight histone proteins. In this work, we investigated the activity of AAG and ALKBH2 on εA lesions globally distributed at positions throughout a strongly positioned NCP. Overall, we examined repair of εA at 23 unique locations in packaged DNA. We observed a strong correlation between rotational positioning of εA and AAG activity, but not ALKBH2 activity. ALKBH2 was more effective than AAG at repairing occluded εA lesions but only AAG was capable of full repair of any εA in the NCP. However, notable exceptions to these trends were observed, highlighting the complexity of the NCP as a substrate for DNA repair. Modeling of binding of the repair enzymes to NCPs revealed that some of these observations can be explained by steric interference caused by DNA packaging. Specifically, interactions between ALKBH2 and the histone proteins obstruct binding to DNA and leads to diminished activity. Taken together, these results support *in vivo* observations of alkylation damage profiles and contribute to our understanding of mutational hotspots.

INTRODUCTION

The DNA lesion 1,N^6-ethenoadenine (εA, Figure 1) is a mutagenic adduct[1] generated by exposure of A to various DNA damaging agents such as vinyl chloride and aldehyde byproducts of lipid peroxidation.[2, 3] Elevated εA levels have been detected in a number of cancerous tissues and in tissues of chronic inflammatory diseases that are associated with future cancer development.[4] The A•T to T•A transversion, possibly induced by εA, is a common mutation observed in the *P53* and *RAS* genes and is associated with carcinogenesis.[5] This carcinogenic effect of εA necessitates a thorough understanding of how cells efficiently repair and remove such damage.

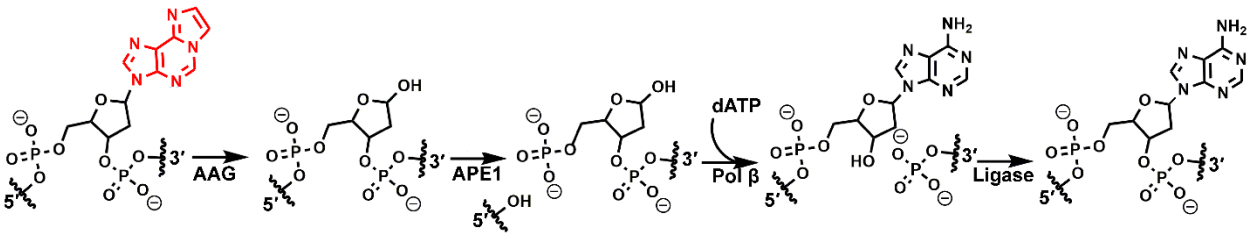

Figure 1. Base excision repair of εA (red) initiated by AAG

The εA lesion is a substrate for two repair pathways: base excision repair (BER) and direct reversal repair (DRR). BER is initiated by a glycosylase removing the lesion (Figure 1), generating an apurinic/apyrimidinic (AP) site.[6] AP endonuclease 1 (APE1) incises the backbone at the AP site generating a nick with 3'-OH and 5'-deoxyribose phosphate (dRP) termini. Polymerase β (Pol β) then removes the dRP group and inserts the correct nucleotide. DNA ligase completes the repair event. In the case of εA, the glycosylase responsible for the removal of εA and some other alkylated lesions is alkyladenine glycosylase (AAG).[7] AAG has been shown to repair alkylated nucleobases in bacteria,[8] yeast,[9] and mammalian cells[10] via a base-flipping mechanism.[11] Furthermore, while

AAG only removes εA from double-stranded substrates, it only requires contact with the lesion-containing strand for substrate recognition.[12]

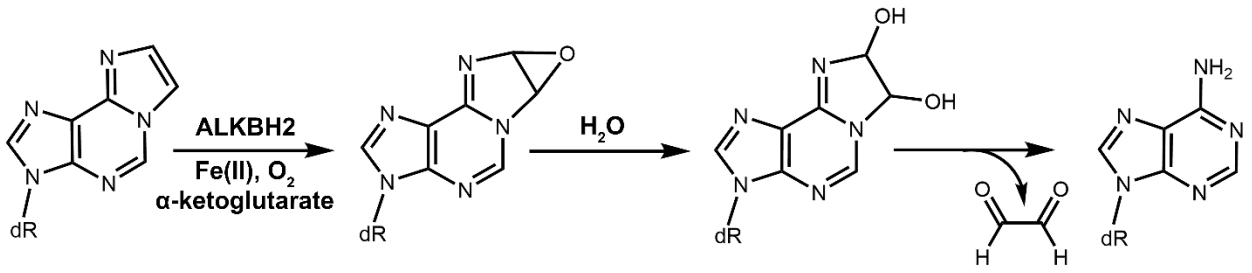

Figure 2. Mechanism of direct repair of εA by the AlkB family of dioxygenases

The removal of εA lesions by DRR is carried out by the AlkB family of dioxygenases, which performs chemistry to directly transform εA to canonical A with a single enzyme (Figure 2).[13-16] Based on sequence homology, up to nine human homologs have been identified as being structurally similar to *E. coli* AlkB.[17] ALKBH2 and ALKBH3 are the enzymes responsible for DRR of εA to A in humans.[18, 19] In particular, ALKBH2 is considered the "housekeeping homolog" responsible for repairing lesions in double-stranded DNA.[20] AlkB homologs are ubiquitous,[21] being observed in RNA viruses,[22] aerobic bacteria,[23] and metazoans.[24] In a manner similar to AAG, ALKBH2 flips its target lesion into its active site prior to chemistry.[25] In contrast to AAG, ALKBH2 requires contact with both strands of DNA to ensure its substrate specificity.[25]

While BER and DRR have been studied extensively in unpackaged DNA, they are not as well understood in the context of chromatin. The nucleosome core particle (NCP) is the basic packaging unit in eukaryotic chromatin and is comprised of 145-147 base pairs of DNA wrapped approximately 1.7 times around a histone protein core.[26] The histone core is formed by two copies of each of the histone proteins H2A, H2B, H3, and H4.[27] Each histone contains a highly structured

globular core and a disordered tail.[26] The NCP also contains a 2-fold axis of pseudosymmetry known as the dyad axis. The location of any nucleobase within the NCP can be characterized according to two parameters: rotational positioning and translational positioning. The rotational positioning of a nucleobase refers to its orientation relative to the histone core and can be defined as outwards towards the solution (OUT), inwards towards the histone core (IN), or a position somewhere in between (MID). The translational position of a nucleobase is based on its distance from the dyad axis. It is known that DNA located further from the dyad axis and closer to the entry-exit points is subject to spontaneous and transient dissociation from the histone core.[28, 29] Furthermore, lesions with different rotational and translational positions exist in varied microenvironments within an NCP which can influence DNA repair. These microenvironments are created by histone tails, DNA superhelical gyres, and transient dissociation of DNA from the histones.

Most literature reports have investigated how AAG and ALKBH2 function on unpackaged DNA substrates. To the best of our knowledge, no work has been reported on DRR in the context of an NCP. The BER and DRR pathways may differ in their ability to work in certain cellular environments, including when DNA is packaged or unpackaged. The overlapping lesion substrates of AAG and ALKBH2 may help balance the need to repair mutagenic lesions against the generation of potentially mutagenic and/or cytotoxic intermediates such as AP sites and nicks. For example, DRR avoids the creation of the AP site generated by BER which has been shown to react with histone lysines leading to a strand break.[30] However, it remains unknown the context in which each repair pathway operates within the cellular environment.

In this study, we used a global population of NCP with εA lesions in a variety of translational and rotational positions to investigate and compare the activities of AAG and

ALKBH2. We utilized a combinatorial approach of hydroxyl radical footprinting (HRF) and enzymatic reactions to evaluate the repair profiles of both AAG and ALKBH2 in strongly positioned nucleosomes (Figure 3). We found that while only AAG has, at some sites, full activity on εA in the NCP, ALKBH2 is better at repairing occluded εA lesions. Through molecular modeling, we hypothesize that these differential repair profiles may be the result of steric interactions with the histone core and some of the structural distortions caused by these two enzymes.

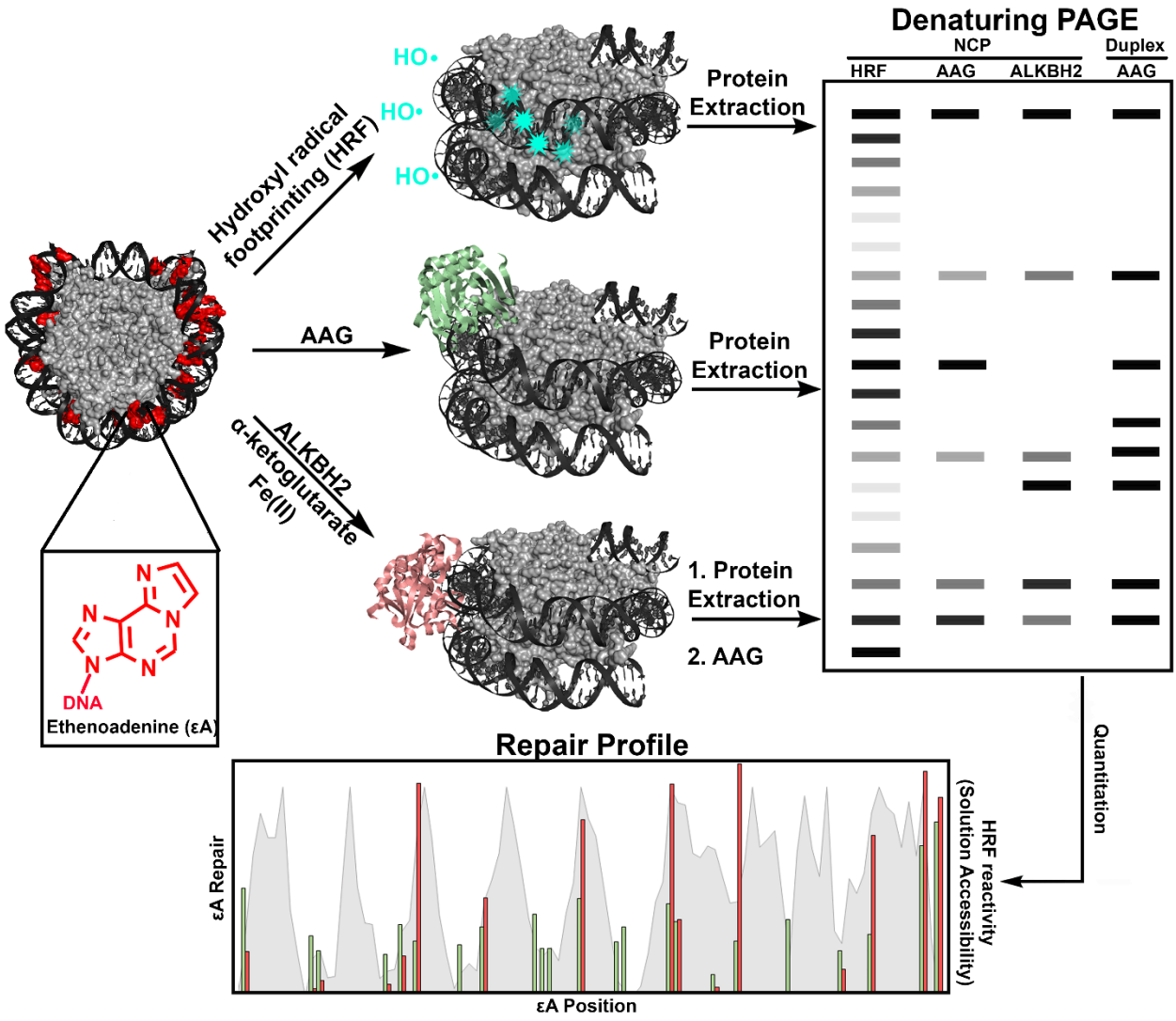

Figure 3. Overall workflow to establish the repair profiles of AAG and ALKBH2 in strongly positioned NCPs. NCPs with εA distributed globally throughout the NCP were assembled. Notably, each NCP contains only a single εA lesion but the population of NCP has εA in a variety of locations. The NCP were treated in three ways. The top shows establishing the solution accessibility of the εA lesions by hydroxyl radical footprinting. The middle shows the treatment of NCPs with AAG to reveal the εA sites that are repaired by BER. The bottom shows the two-step process for revealing DRR by ALKBH2. First, the NCPs are treated with ALKBH2 and its cofactors. The histone proteins are then extracted and the liberated DNA is treated with AAG to reveal sites that were not repaired, and by comparison to controls, the εA sites that were repaired by ALKBH2. The data is quantitated and combined to reveal the repair profile of εA in strongly positioned NCPs.

MATERIALS AND METHODS

Oligonucleotide Synthesis and Purification

All oligonucleotides used in this study were synthesized on a MerMade 4 DNA synthesizer (BioAutomation). All reagents were purchased from Glen Research. We used the 145 bp Widom 601 nucleosome positioning sequence (Scheme S1) as the unincorporated duplex control and to assemble NCP. Base pairs are numbered starting with the first base of the 5′-end of the "I" strand. The 145 mer oligonucleotide containing εA was synthesized on 1,400 Å controlled pore glass beads using phosphoramidites with ultramild protecting groups and deprotected according to the manufacturer's specifications. A Poisson distribution was utilized to substitute εA for A throughout the "I" strand, similar to recent reports.[31-33] We accomplished this distribution by using an εA and A phosphoramidite mixture during the synthesis, with the molar ratio determined by the Poisson distribution ($\lambda = 0.355$). The resulting DNA population contains either 0 or 1 εA lesion per 145 mer oligonucleotide with only 5% containing two or more lesions. The DNA was cleaved from the beads by incubation in NH_4OH at room temperature for 2 h. The DNA was then purified by 8% denaturing polyacrylamide gel electrophoresis (PAGE).

The complementary 145 mer was prepared using a ligation strategy (Scheme S2). The component oligonucleotides for ligation were synthesized using standard phosphoramidite protecting groups and the final trityl group was retained. Reverse-phase HPLC purification at 90 °C was used to purify the oligonucleotides with a trityl group (Agilent PLRP-S column, 250 mm × 4.6 mm; A = 100 mM triethylammonium acetate [TEAA] in 5% aqueous MeCN, B = 100 mM TEAA in MeCN; 5:95 to 35:65 of A:B over 30 min, 35:65 to 5:95 of A:B over 5 min at 1 mL/min, retention times ranged from 24-29 min). Incubation in 20% v/v aqueous glacial acetic acid for 1 h

at room temperature removed the trityl group and a second HPLC purification at 90 °C was performed (Agilent PLRP-S column, 250 mm × 4.6 mm; A = 100 mM triethylammonium acetate [TEAA] in 5% aqueous MeCN, B = 100 mM TEAA in MeCN; 0:100 to 15:85 of A:B over 35 min, 15:85 to 35:65 of A:B over 5 min at 1 mL/min, retention times ranged from 28-32 min). Electrospray ionization mass spectrometry was used to verify the identity of the component oligonucleotides. Five nmol of each component oligonucleotide J2 and J3 (Scheme S2) were 5′-phosphorylated using 2 mM ATP and 30 U T4 kinase (New England Biolabs). These phosphorylated components were then combined in equal molar amounts with component J1 and 10% excess of two scaffolding oligonucleotides, JS12 and JS23, and annealed by heating to 95°C for 5 min and cooling at 1°C per min to room temperature in 50 mM NaCl and 20 mM Tris (pH 8.0). These annealed oligonucleotides were then ligated at room temperature overnight using 4,800 U T4 DNA ligase (New England Biolabs). The product of the ligation reaction was then purified using 8% denaturing PAGE.

The two single-stranded internal standards, used for normalizing band quantification in the AAG and ALKBH2 analyses, were designed as a 23 mer and a 92 mer (Scheme S1) such that they would not co-migrate with any εA cleavage product. They were synthesized as described above and purified by 12% and 8% denaturing PAGE, respectively.

Reconstitution of Global εA Nucleosome Core Particles

Recombinant *Xenopus laevis* histones were individually expressed and purified, and subsequently assembled into octamers.[34, 35] NCPs were reconstituted by dialyzing the radiolabeled εA-containing duplex population and histone octamer together via salt gradient, as described previously.[34] Briefly, a 7% molar excess of histone octamer (0.54 μM octamer) was added to

radiolabeled εA containing 145 bp duplex (0.5 μM DNA) in buffer (10 mM Tris-HCl [pH 7.5], 1 mM EDTA, 1 mM dithiothreitol [DTT], 2 M NaCl, 500 μg/mL BSA) in a Slide-a-Lyzer dialysis device (0.1 mL capacity, 3.5 kDa MWCO; Thermo Fisher Scientific). The dialysis device started in a buffer of 10 mM Tris-HCl (pH 7.5), 1 mM EDTA, 1 mM DTT, 2 M NaCl at 4 °C. The device was placed in buffers containing decreasing concentrations of NaCl (1.2 M, 1.0 M, 0.6 M, 0 M) at hourly intervals. The final dialysis proceeded for 3 h and then the NCPs were filtered with a 0.22 μm cellulose acetate centrifuge tube filter (Corning Costar) to remove insoluble particles. NCP formation and relative purity were analyzed using a 7% native PAGE (60:1 acrylamide:bisacrylamide; 0.25x TBE) run for 3 h at 160 V at 4 °C (Figure S1). Only NCPs containing ≤ 5% duplex DNA were used in further studies.

Hydroxyl Radical Footprinting

Hydroxyl radical footprinting was utilized to determine the relative solution accessibility of nucleobases in the NCP. A modified version of the method of Tullius[36, 37] was used to ensure single-hit conditions. Briefly, 7.5 μL of each 1 mM Fe(II)-EDTA, 10 mM sodium ascorbate, and 0.12% w/v aqueous hydrogen peroxide were combined with 5 pmol NCPs in 52.5 μL buffer (10 mM Tris-HCl [pH 7.5], 1 mM EDTA). This mixture was incubated in the dark at room temperature for 10 min and then quenched with 16 μL 1 mM EDTA in 25% v/v glycerol. This quenched sample was immediately loaded onto a 7% native PAGE (60:1 acrylamide:bisacrylamide; 0.25x TBE) and run for 3 h at 155 V at 4 °C. The gel bands containing NCPs were excised and eluted into buffer (0.3 M NaOAc, 1 mM Tris-HCl [pH 8.0], 1 mM EDTA) for 18-24 h at 37°C with gentle shaking (60 rpm). The eluent was then concentrated using a centrifugal concentrator (Sartorius Viaspin Turbo 15, 5 kDa MWCO) and filtered using a 0.22 μm cellulose acetate syringe filter. The samples was extracted with equal volume addition of 25:24:1 phenol:chloroform:isoamyl alcohol (PCI)

and the aqueous layer was concentrated by SpeedVac evaporation. Following the addition of 40 µL co-precipitation agent (0.5 mg/mL tRNA in 300 mM NaOAc [pH 8.0], 1 mM EDTA), samples were desalted with ethanol precipitation. Samples were resuspended in a 1:1 mixture of formamide and water for denaturing PAGE. Cleavage fragments were resolved by 8% denaturing PAGE (Figure S2) and quantitated using SAFA[38] gel analysis software. The determination of solution accessibilities of nucleobases was achieved by normalization to the highest band intensity within a helical turn (Table S1). Briefly, the band intensities were plotted against base position to identify the peaks and valleys corresponding to OUT and IN locations respectively. The identified peaks with the highest band intensity were assigned as the most OUT position within a helical turn and assigned a value of 1. The band intensity of the five bases flanking each side of this OUT position were then normalized to this value to give the solution accessibility within the helical turn. This normalization allows for direct comparison of rotational positioning throughout all bases in the NCP. Highly solution-accessible (OUT) positions were defined as those with a ratio greater than or equal to 0.7; medium solution-accessible (MID) positions with a ratio range from 0.3-0.7; low solution accessibility (IN) positions were defined as those with a ratio less than 0.3.

Enzymatic Reactions

Human AAG was purchased from New England Biolabs, and the total enzyme concentration was determined by Bradford assay using γ-globulin standards (Bio-Rad Laboratories). Human ALKBH2 was expressed, purified and quantified as previously described.[39, 40] To assess the activity of ALKBH2 or AAG, 1 pmol substrate (either duplex DNA or NCPs) were mixed with 40 pmol ALKBH2 or AAG in a total volume of 20 µL of the reaction buffer (20 mM Tris, 50 mM NaCl, 150 mM KCl, 1 mM DTT, 100 µg/mL BSA, 1.5 mM α-ketoglutarate disodium salt, 3 mM sodium ascorbate, 50 mM HEPES (pH 8), and 100 µM

$Fe(NH_4)_2(SO_4)_2•(H_2O)_6$). The reaction buffer was the same for both enzymes to ensure a direct comparison of repair with the same biophysical characteristics of the NCP in each instance. The samples were incubated for 1 h at 37 °C along with a negative control sample (no enzyme). After the incubation, AAG treated samples were quenched with 20 μL of 1M NaOH which had been spiked with the radiolabeled internal standards and heated to at 90 °C for 3 min. The internal standards were added based on counts. The counts per each εA site was determined ([total number of counts × 0.25 (since 25% of DNA contains εA]/33 (total number of εA sites) and multiplied by 1.7 to define how many counts of each internal standard was added. ALKBH2 treated samples were quenched with a final concentration 25 mM EDTA and heated at 95 °C for 5 min. For both the AAG and ALKBH2 samples, the protein and DNA were then separated using an extraction with PCI. For AAG treated samples, the aqueous layer was supplemented with 40 μL co-precipitation agent (0.5 mg/mL tRNA in 300 mM NaOAc [pH 8.0], 1 mM EDTA) and 600 μL ethanol before being placed on dry ice for 30 min. For the ALKBH2 treated samples, the aqueous phase was supplemented with 40 μL 0.5 M sodium acetate and 600 μL ethanol and placed on dry ice for 30 min. The ALKBH2 treated samples were then reconstituted in 20 mM Tris (pH 8.0), 50 mM NaCl, 150 mM KCl, 1 mM DTT, 100 μg/mL BSA, 40 pmol of AAG was added, and the sample was incubated for 1 h at 37 °C. Another sample was kept as a negative control to reveal background damage during workup and was not treated with AAG. These samples were then quenched by 0.5 M NaOH, heated to 90 °C for 3 min. These samples were then supplemented with 40 μL co-precipitation agent (0.5 mg/mL tRNA in 300 mM NaOAc [pH 8.0], 1 mM EDTA) and 600 μL ethanol before being placed on dry ice for 30 min. All samples were resuspended in 50% v/v formamide:water, split in half, and loaded onto an 8% gel (Figure S3). One half of the samples

were loaded to resolve bands 19-64, run 2 h at 80 W. The other half of the samples were loaded to resolve of bands 89-132, run 4 h at 80 W.

The gels were visualized by phosphorimagery and the bands were quantified using SAFA software. The band intensities were normalized using the internal standards. Sites 19-64 were normalized with the 23 mer standard, and sites 89-132 were normalized using the 92 mer standard. The no enzyme control was used to subtract background from enzyme-treated samples. For each site, the ratio of corrected band intensity in the NCPs to the duplex was used to determine the NCP/Duplex (NCP/DUP) ratio for AAG activity. An NCP/DUP value of 1 indicates activity that is comparable to duplex, while a value below one indicates lower activity relative to duplex. As a result of εA repair to A by ALKBH2, the DNA is no longer a substrate for AAG and does not generate a strand break under strongly basic conditions. Thus, we measured the loss of density in bands in ALKBH2-treated samples as compared to AAG only treatments. As ALKBH2 activity increased, we found that there was a corresponding drop in band density after AAG treatment. For ALKBH2, a value of 1 indicates a lack of repair while a value lower than 1 indicates repair by ALKBH2. To allow a direct comparison to AAG, this NCP/DUP value was then subtracted from 1 to convert to ALKBH2 repair. The standard error (SE) of NCP/DUP was calculated using $SE = \sigma/\sqrt{(n)}$, where σ is the standard deviation of the population and n is the sample size. For both AAG and ALKBH2, sites 19-123, n=5 and for sites 130 and 132, n=3.

Molecular Modeling

Molecular models were used to approximate enzyme binding to NCPs. The crystal structure of DNA-bound AAG (PDB: 1EWN, resolution 2.1 Å) or ALKBH2 (PDB 3RZK, resolution 2.8 Å) were aligned with the NCP crystal structure (PDB: 3LZ0, resolution 2.5 Å) using

PyMOL. The alignment was performed using the phosphate atoms of the five base pairs on either side of the lesion aligned with the five base pairs on either side of the site of interest (either site 42 or 64) using the "pair_fit" function of PyMOL. Color ramps were then applied to the surface representation of each enzyme to map the proximity to the histone core.

RESULTS

Preparation of NCP Containing Globally Substituted εA Lesions

To investigate the εA repair profiles of AAG and ALKBH2, we prepared NCPs using the Widom 601 DNA sequence.[41] The 601 sequence is a strong positioning sequence which binds the histone octamer in a single translational and rotational position and provides a homogeneous population of NCPs for repair studies. Crystal structures of the 601 NCP are also available for reference.[41] Using methods we reported previously,[31-33] εA lesions were incorporated at A sites in the "I" strand of the 601 DNA to create εA:T base pairs throughout the sequence. We utilized a Poisson distribution to determine the molar ratio of A to εA building blocks such that 95% of the synthesized DNA sequences contain no more than one εA.

Rotational Position of DNA in NCP

We utilized HRF to establish the rotational position of each nucleobase and εA lesion.[37] The hydroxyl radical abstracts preferentially the C5' hydrogen of the sugar-phosphate backbone, which is located in the minor groove. For DNA packaged in NCPs, the regions of most intense strand cleavage indicate that the minor groove is solvent exposed and, thus, the major groove is facing the histone core and is protected from hydroxyl radicals. Therefore, a characteristic of DNA

packaged in NCPs is an oscillating pattern of high and low reactivity towards hydroxyl radicals. This pattern is observed in Figure S2.

Quantitation of the HRF confirms variable levels of solution accessibility throughout the DNA (Table S1). At OUT sites, defined here as having solution accessibility of greater than or equal to 0.7 when normalized within a helical turn, nucleobases are most solution accessible to hydroxyl radicals. The IN sites are defined as having solution accessibility less than 0.3; these sites are the least susceptible to cleavage by hydroxyl radicals because they are protected by the proximity of the histone proteins. The MID sites have solution accessibility between 0.3 and 0.7, exhibiting moderate protection by the histone proteins. The εA lesions are in a variety of rotational and translational positions that allows for a global analysis of the effects of geometric position on repair. Of the εA sites evaluated in this work, 8 are OUT, 4 are MID, and 11 are IN; these 23 lesion sites are also distributed throughout various translation positions in the NCP.

Excision Activity of AAG in NCP Correlates with Rotational Position

AAG is known to remove εA from duplex DNA that is not incorporated into an NCP (unincorporated duplex).[42-44] Therefore, at each εA site, the ratio of excision from NCP relative to unincorporated duplex (NCP/DUP) is plotted (Figure 4A, striped bars). A ratio of 1 reflects comparable excision activity in NCP and unincorporated duplex DNA. We find that AAG glycosylase activity in NCP correlates strongly with rotational position (Figure 4B, open circles), in agreement with previous reports.[31] Most OUT sites (42, 64, 96, 123, 130, 132) exhibit high AAG activity as defined by NCP/DUP > 0.6. The only notable exceptions are sites 97 and 102 where relatively low levels of excision below 0.4 are observed in NCP. Consistent with the correlation between rotational position and excision activity, IN sites (19, 38, 48, 58, 59, 89, 90,

112) exhibit low AAG activity with NCP/DUP < 0.2. AAG exhibits a wider range of activity at MID sites with most NCP/DUP ranging from 0.1-0.6. However, site 105 exhibits a much higher activity, reaching 1. Furthermore, sites located towards the 3′-end of the "I" strand, near the DNA entry/exit region, generally exhibit higher levels of AAG activity than observed at other locations in the NCP. Importantly, native PAGE analysis demonstrates that NCPs remain intact after incubation with AAG and that the glycosylase does not act by removing DNA from histones.

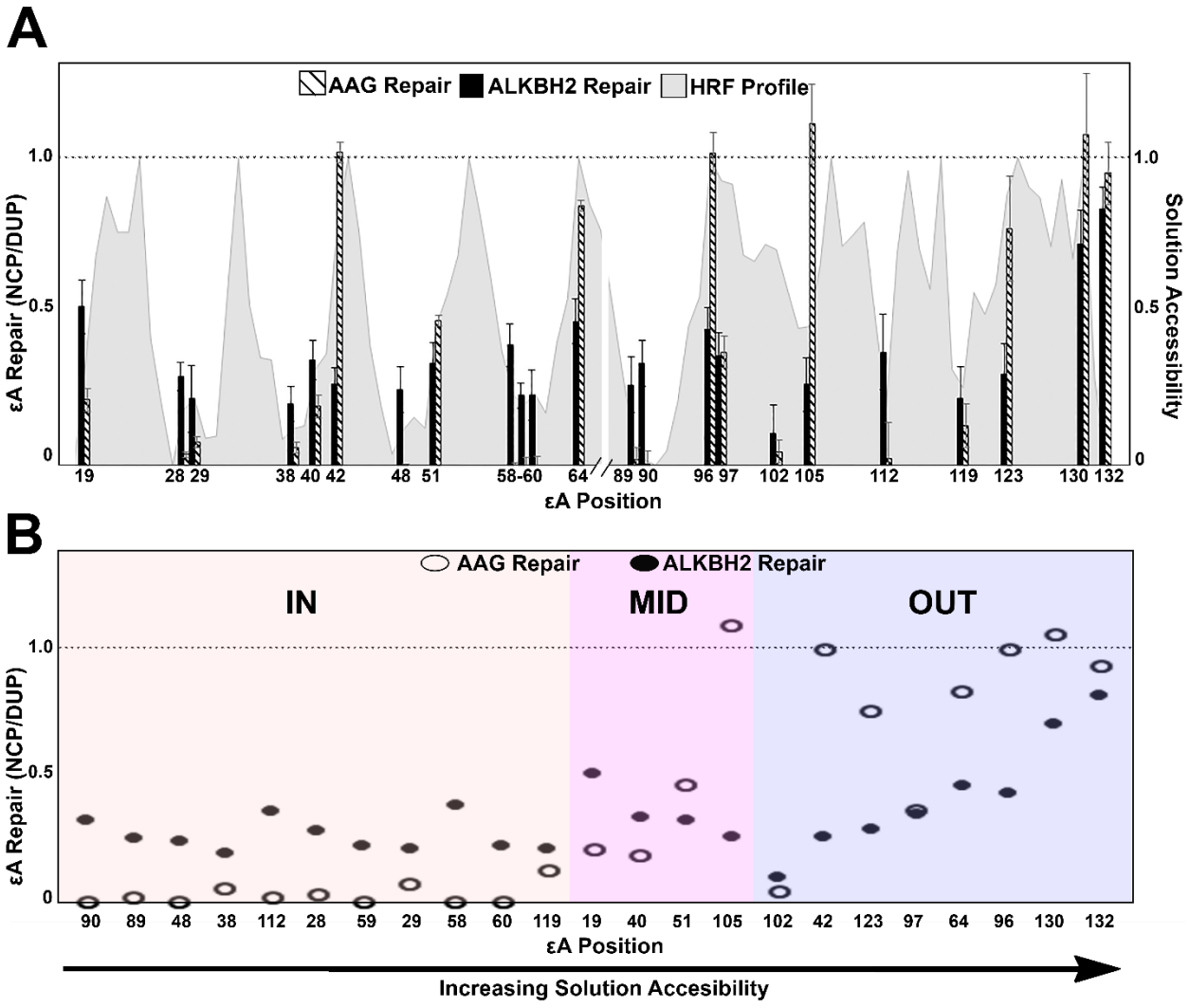

Figure 4. Repair profiles for AAG and ALKBH2. **(A)** The amount of εA excision for AAG (striped bars) and repair by ALKBH2 (solid bars) are plotted with solution accessibility as established by HRF (gray area) **(B)** Excision of εA by AAG (open circles) and repair by ALKBH2 (solid circles) plotted as a function of increasing solution accessibility.

Repair of εA by ALKBH2 is Unhindered in Duplex DNA but Suppressed in NCP

The ability of ALKBH2 to repair εA was markedly different between unincorporated duplex and NCP. εA was repaired at all 23 sites evaluated in unincorporated duplex, with all εA lesions repaired at least 70% (Figure S4). In contrast, only sites 19, 130, and 132 in the NCP have NCP/DUP ≥ 0.5 and no εA lesions are repaired as readily as in unincorporated duplex (Figure 4A, black bars). Furthermore, while OUT sites (such as sites 42, 64, and 96) show somewhat higher repair activity than MID or IN sites, this correlation with rotational position is much weaker than observed for AAG and was not observed at all OUT sites (Figure 4B, black circles). It is notable that at site 97, the decrease in activity for AAG upon incorporation of the DNA into an NCP is not observed for ALKBH2 and, therefore, direct repair is comparable to AAG excision at this OUT site. In comparison to AAG, ALKBH2 exhibits greater activity at IN sites with all 11 IN sites exhibiting NCP/DUP ≥ 0.2. However, none of these IN sites reached NCP/DUP ≥ 0.4. Similar to AAG, native PAGE analysis demonstrates that NCPs remain intact after incubation with ALKBH2.

ALKBH2 Exhibits Greater Steric Interactions with the Histone Core than AAG

The εA lesions at OUT sites 42 and 64 were chosen for more in depth molecular modeling because despite having the same rotational orientation, AAG exhibits higher repair activity at site 42, while ALKBH2 has higher repair at site 64. Our enzyme docking analysis shows that for sites

42 and 64, steric influences play a pronounced role in enzymatic activity, particularly for ALKBH2 (Figure 5). Minimal steric clash is observed between the histone core and AAG when binding at site 42 where excision of εA is complete as evidenced by the near lack of yellow and red in the proximity map (Figure 5D, top). In fact, no AAG amino acid residues are within 5 Å of the histone octamer at site 42. In comparison, a steric clash between the histone core and AAG is seen when AAG is docked at site 64 as observed by the 13 amino acid residues within 5 Å of the histone core (Figure 5D, bottom); notably, AAG still demonstrates a NCP/DUP of 0.84.

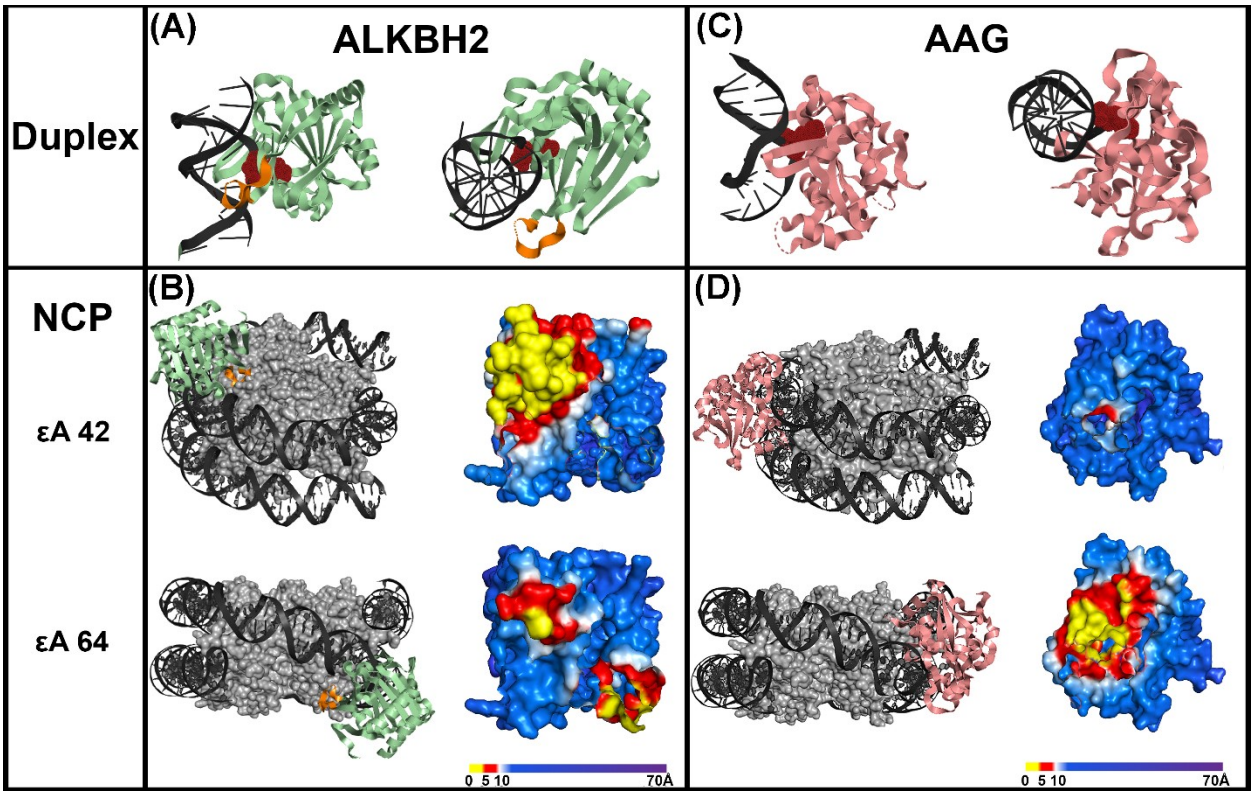

Figure 5. Molecular modeling of steric interactions between ALKBH2 and AAG upon substrate binding. **(A)** ALKBH2-duplex co-crystal structure (PDB: 3RZK) (left is side view; right is view down helical axis of DNA). εA is in red and can be seen flipped into the active site. The long loop is highlighted in orange. **(B)** ALKBH2-duplex co-crystal structure (PDB: 3RZK) merged with the NCP (PDB: 3LZ0) at εA sites 42 (top) and 64 (bottom). ALKBH2 surface models are rotated and enlarged to show the NCP binding face and colored according to the distance to the histone core. Amino acids within 5 Å of the histones are in yellow, those between 5 and 10Å are in red, and further distances are in blue. **(C)** AAG-duplex co-crystal structure (PDB: 1EWN) (left is side view; right is view down helical axis of DNA). εA is in red and can be seen flipped into the active site. **(D)** AAG-duplex co-crystal structure (PDB: 1EWN) merged with the NCP (PDB: 3LZ0) at εA sites 42 (top) and 64 (bottom). AAG surface models are rotated and enlarged to show the NCP binding face and colored according to the distance to the histone core.

In contrast, ALKBH2 has a NCP/DUP of only 0.25 at site 42 where there is substantial steric clash of 15 amino acid residues within 5 Å of the octamer core, all residing within the long loop of ALKBH2 (Figure 5B, top).[25] At site 64, where there is only a single amino acid from the long loop within 5 Å of the histones although another region of the enzyme has steric interactions with the histones (Figure 5B, bottom), there is enhanced repair activity that increases NCP/DUP to 0.40.

DISCUSSION

In this work, we compare the global repair profiles of AAG and ALKBH2 acting on εA lesions distributed throughout a strongly positioned NCP, encompassing different microenvironments with varying geometric positions. As observed previously, εA removal by AAG is highly correlated with rotational position.[31] This result is consistent with the general trend that has been observed previously for other glycosylases acting on strongly positioned NCPs. We have reported that OGG1,[33, 45] UDG,[32, 45] TDG,[46] and AAG[31, 45] exhibit activity at sites facing OUT from the histone core. These findings are also consistent with results reported by other groups.[47-

[50] An alternate approach to repair εA lesions is DRR by the AlkB family enzymes. Overall, we found substantial inhibition of ALKBH2 across the NCP, even at OUT sites. Intriguingly, all but one IN site (site 28) exhibit higher activity by ALKBH2 than AAG, albeit modest activity. These data suggest that while the ALKBH2 repair is more broadly inhibited in NCPs compared to AAG, ALKBH2 has higher activity on occluded sites that are poorly excised by AAG. Notably, ALKBH2 does not greatly distort DNA upon binding (Figure 5A) and may be easier to accommodate than the 22° angle pinching of the DNA observed for AAG[12] (Figure 5C, left). We hypothesize that the lesser degree of distortion of the DNA helix by ALKBH2 leads to its higher activity at occluded sites compared to AAG. However, neither enzyme demonstrates an ability to completely repair occluded lesions, indicating that these sites may represent mutational hotspots in the absence of structural changes to the NCP or external factors to enhance accessibility.

Our NCP system with εA in a variety of positions also allows us to consider the role of DNA sequence context on the activity of AAG and ALKBH2. We did not observe any significant sequence context effects for either AAG or ALKBH2, although it should be noted that these results are not a comprehensive study of all possible sequence contexts of εA (Table S2). This result is consistent with previous reports of AAG excision of εA being independent of sequence context.[11] Rather than sequence context, the rotational orientation of εA seems to be the dominant factor in predicting both enzymes' ability to initiate repair.

Modelling of AAG and ALKBH2 docked at OUT sites provides insight into binding of these two enzymes to NCP substrates. Steric interactions between the histone core and the long loop of ALKBH2 (Figure 5, highlighted in orange), which is known to play an essential role in substrate binding,[25] modulate binding to the NCP. The stronger steric interactions with the long

loop at OUT sites lead to diminished ALKBH2 activity as can be seen by comparing sites 42 and 64. Notably, this modeling does not account for the dynamic histone tails that could also modulate binding of repair enzymes. It is intriguing to consider that the H2B and H4 tails near site 97 may contribute to the unexpectedly low amount of excision by AAG at this location as histone tails have been shown to alter the structure and dynamics of damaged DNA.[51, 52] The H2B tail is also in close proximity to site 102 and may account for the unexpected lower levels of εA excision by AAG. However, the unexpectedly high excision at site 105 indicates that the microenvironment generated by the H2B tail may have more complex and nuanced effects that include local structural changes, sterics, and electrostatics. These effects may be beneficial or inhibitory for different nucleobases that exist in a similar microenvironment.

DNA located near the entry/exit region of the NCP is known to transiently and spontaneously unwrap and expose otherwise occluded lesion sites. In particular, the 3′-end of the Widom 601 "I" strand has been shown to unwrap preferentially.[53] The high levels of activity for both enzymes at sites 123, 130, and 132 is likely due to this asymmetric unwrapping. While the kinetics of unwrapping have not been measured in the presence of a DNA binding enzyme, the histone chaperone Nap1 has been shown to exploit unwrapping to promote H2A-H2B dimer eviction.[54] Furthermore, it has been demonstrated that unwrapping is rate-limiting for endonuclease III-like protein 1 (NTH1).[55, 56] These results agree with our earlier reports that solution accessibility does not correlate with glycosylase activity in certain translational regions.[32, 33, 45] Specifically, excision of uracil by UDG[32] and excision of 8-oxo-7,8-dihydroguanine by OGG1[33] are enhanced at the DNA entry/exit regions and was attributed to the unwrapping of the DNA. However, this observation is not universal and is dependent upon the specific glycosylase,

as NEIL1 has been reported to be unable to exploit this unwrapping due to its high affinity for undamaged bases.[55]

Our results are also consistent with reports that demonstrated accumulation of alkylation damage in yeast at IN sites in genomic DNA.[57] Decreased repair at these sites is further indicated in an analysis of human tumors, in which mutational hotspots were observed at IN sites.[58] Taken together these data suggest that an alternate means of accessing occluded lesions, such as chromatin remodelers or histone modifications, may be required. Indeed, H2B[59] and H3[60] acetylation has been shown to enhance DNA unwrapping and acetylation has been observed to occur as part of the DNA damage response.[61] Furthermore, incorporation of histone variants has been demonstrated to enhance the initiation of BER of uracil lesions.[32] Finally, it was recently shown that AAG forms a complex with RNA polymerase II and may utilize localized chromatin decondensation to access otherwise occluded lesions.[62]

Further understanding of the molecular mechanisms of εA repair is essential to understand and inform clinical impacts. Abnormal expression of both AAG and ALKBH2 have been observed in cancer pathologies. Overexpression of AAG has been associated with both decreased sensitivity to various chemotherapeutic agents in mouse embryonic stem cells and increased sensitivity in breast cancer cells.[10, 63] ALKBH2 also has clinical significance, as its knockdown in bladder cancer tissues limited tumor development, while downregulation led to increased sensitivity to alkylating agents and chemotherapeutics.[64] The potential for AlkB homolog inhibitors to serve as anticancer agents has also been investigated.[40] However, the potential obstacles to the activity of these enzymes, such as the packaging of DNA into the NCP, need to be better understood to inform future therapies.

ASSOCIATED CONTENT

Supporting Information

The Supporting Information is available free of charge on the ACS Publications website.

DNA sequences and schemes, supplementary figures and tables (including gel images, ALKBH2 duplex treatment quantification, hydroxyl radical footprinting, and normalized HRF reactivity values).

AUTHOR INFORMATION

Corresponding Author

*Email: sarah_delaney@brown.edu. Phone: +1 401 863 1000.

Funding

This research was supported by the National Science Foundation (MCB-1817417 to S.D.) and National Institutes of Health (R15 CA213042 and R01 ES028865 to D.L.).

Notes

The authors declare no competing financial interest.

ACKNOWLEDGMENT

We thank members of the Delaney laboratory for helpful discussion and Dr. Erin Kennedy for discussion and critical reading of the manuscript.

REFERENCES

1. Levine, R. L.; Yang, I.-Y.; Hossain, M.; Pandya, G. A.; Grollman, A. P.; Moriya, M. (2000) Mutagenesis induced by a single 1,*N6*-ethenodeoxyadenosine adduct in human cells. *Cancer Res. 60* (15), 4098-4104.
2. El Ghissassi, F.; Barbin, A.; Nair, J.; Bartsch, H. (1995) Formation of 1,*N6*-ethenoadenine and 3,*N4*-ethenocytosine by lipid peroxidation products and nucleic acid bases. *Chem. Ress. Toxicol. 8* (2), 278-283.
3. Guengerich, F. P.; Crawford, W. M.; Watanabe, P. G. (1979) Activation of vinyl chloride to covalently bound metabolites: roles of 2-chloroethylene oxide and 2-chloroacetaldehyde. *Biochemistry 18* (23), 5177-5182.
4. Nair, U.; Bartsch, H.; Nair, J. (2007) Lipid peroxidation-induced DNA damage in cancer-prone inflammatory diseases: A review of published adduct types and levels in humans. *Free Radic. Biol. Med. 43* (8), 1109-1120.

5. Barbin, A. (200) Etheno-adduct-forming chemicals: from mutagenicity testing to tumor mutation spectra. *Mutat. Res. Rev. Mutat.*, *462* (2), 55-69.
6. Schermerhorn, K. M.; Delaney, S. (2014) A chemical and kinetic perspective on base excision repair of DNA. *Acc. Chem. Res. 47* (4), 1238-1246.
7. O'Brien, P. J.; Ellenberger, T. (2004) Dissecting the broad substrate specificity of Human 3-Methyladenine-DNA Glycosylase. *J. Biol. Chem. 279* (11), 9750-9757.
8. Ayala-García, V. M.; Valenzuela-García, L. I.; Setlow, P.; Pedraza-Reyes, M. (2016) Aag hypoxanthine-DNA glycosylase is synthesized in the forespore compartment and involved in counteracting the genotoxic and mutagenic effects of hypoxanthine and alkylated bases in DNA during *Bacillus subtilis* Sporulation. *J. Bacteriol.198* (24), 3345-3354.
9. Glassner, B. J.; Rasmussen, L. J.; Najarian, M. T.; Posnick, L. M.; Samson, L. D. (1998) Generation of a strong mutator phenotype in yeast by imbalanced base excision repair. *Proc. Natl. Acad. Sci. U.S.A. 95* (17), 9997-10002.
10. Allan, J. M.; Engelward, B. P.; Dreslin, A. J.; Wyatt, M. D.; Tomasz, M.; Samson, L. D. (1998) Mammalian 3-methyladenine DNA glycosylase protects against the toxicity and clastogenicity of certain chemotherapeutic DNA cross-linking agents. *Cancer Res.*, *58* (17), 3965-3973.
11. Wolfe, A. E.; O'Brien, P. J. (2009) Kinetic mechanism for the flipping and excision of 1,N(6)-ethenoadenine by human alkyladenine DNA glycosylase. *Biochemistry 48* (48), 11357-11369.
12. Lau, A. Y.; Scharer, O. D.; Samson, L.; Verdine, G. L.; Ellenberger, T. (1998) Crystal structure of a human alkylbase-DNA repair enzyme complexed to DNA: mechanisms for nucleotide flipping and base excision. *Cell 95* (2), 249-58.
13. Aravind, L.; Koonin, E. V. (2001) The DNA-repair protein AlkB, EGL-9, and leprecan define new families of 2-oxoglutarate- and iron-dependent dioxygenases. *Genome Biol. 2* (3), research0007.1.
14. Sedgwick, B. (2004) Repairing DNA-methylation damage. *Nat. Rev. Mol. Cell Biol. 5* (2), 148-157.
15. Delaney, J. C.; Smeester, L.; Wong, C.; Frick, L. E.; Taghizadeh, K.; Wishnok, J. S.; Drennan, C. L.; Samson, L. D.; Essigmann, J. M. (2004) AlkB reverses etheno DNA lesions caused by lipid oxidation in vitro and in vivo. *Nat. Struct. Mol. Biol. 12* (10), 855-860.
16. Mishina, Y.; Yang, C.-G.; He, C. (2005) Direct repair of the exocyclic DNA adduct 1,N6-ethenoadenine by the DNA repair AlkB proteins. *J. Am. Chem. Soc. 127* (42), 14594-14595.
17. Ougland, R.; Rognes, T.; Klungland, A.; Larsen, E. (2015) Non-homologous functions of the AlkB homologs. *J. Mol. Cell Biol. 7* (6), 494-504.
18. Aas, P. A.; Otterlei, M.; Falnes, P. Ø.; Vågbø, C. B.; Skorpen, F.; Akbari, M.; Sundheim, O.; Bjørås, M.; Slupphaug, G.; Seeberg, E.; Krokan, H. E. (2003) Human and bacterial oxidative demethylases repair alkylation damage in both RNA and DNA. *Nature 421* (6925), 859-863.
19. Duncan, T.; Trewick, S. C.; Koivisto, P.; Bates, P. A.; Lindahl, T.; Sedgwick, B. (2002) Reversal of DNA alkylation damage by two human dioxygenases. *Proc. Natl. Acad. Sci. U.S.A 99* (26), 16660-16665.
20. Ringvoll, J.; Nordstrand, L. M.; Vågbø, C. B.; Talstad, V.; Reite, K.; Aas, P. A.; Lauritzen, K. H.; Liabakk, N. B.; Bjørk, A.; Doughty, R. W.; Falnes, P. Ø.; Krokan, H. E.;

Klungland, A. (2006) Repair deficient mice reveal mABH2 as the primary oxidative demethylase for repairing 1meA and 3meC lesions in DNA. *EMBO J. 25* (10), 2189-2198.
21. Fedeles, B. I.; Singh, V.; Delaney, J. C.; Li, D.; Essigmann, J. M. (2015) The AlkB Family of Fe(II)/alpha-ketoglutarate-dependent dioxygenases: repairing nucleic acid alkylation damage and beyond. *J. Biol. Chem* (34), 20734-42.
22. van den Born, E.; Omelchenko, M. V.; Bekkelund, A.; Leihne, V.; Koonin, E. V.; Dolja, V. V.; Falnes, P. Ø. (2008) Viral AlkB proteins repair RNA damage by oxidative demethylation. *Nucleic Acids Res. 36* (17), 5451-5461.
23. Sedgwick, B.; Bates, P. A.; Paik, J.; Jacobs, S. C.; Lindahl, T. (2007) Repair of alkylated DNA: Recent advances. *DNA Repair 6* (4), 429-442.
24. Drabløs, F.; Feyzi, E.; Aas, P. A.; Vaagbø, C. B.; Kavli, B.; Bratlie, M. S.; Peña-Diaz, J.; Otterlei, M.; Slupphaug, G.; Krokan, H. E. (2004) Alkylation damage in DNA and RNA—repair mechanisms and medical significance. *DNA Repair 3* (11), 1389-1407.
25. Yang, C.-G.; Yi, C.; Duguid, E. M.; Sullivan, C. T.; Jian, X.; Rice, P. A.; He, C. (2008) Crystal structures of DNA/RNA repair enzymes AlkB and ABH2 bound to dsDNA. *Nature 452* (7190), 961-965.
26. Luger, K.; Mäder, A. W.; Richmond, R. K.; Sargent, D. F.; Richmond, T. J. (1997) Crystal structure of the nucleosome core particle at 2.8 Å resolution. *Nature 389* (6648), 251-260.
27. Eickbush, T. H.; Moudrianakis, E. N. (1978) The histone core complex: an octamer assembled by two sets of protein-protein interactions. *Biochemistry 17* (23), 4955-4964.
28. Lee, J. Y.; Lee, J.; Yue, H.; Lee, T. H. (2015) Dynamics of nucleosome assembly and effects of DNA methylation. *J. Biol. Chem 290* (7), 4291-303.
29. Zhou, K.; Gaullier, G.; Luger, K. (2019) Nucleosome structure and dynamics are coming of age. *Nat. Struct. Mol. Biol. 26* (1), 3-13.
30. Sczepanski, J. T.; Wong, R. S.; McKnight, J. N.; Bowman, G. D.; Greenberg, M. M. (2010) Rapid DNA–protein cross-linking and strand scission by an abasic site in a nucleosome core particle. *Proc. Natl. Acad. Sci. U.S.A 107* (52), 22475-22480.
31. Kennedy, E. E.; Li, C.; Delaney, S. (2019) Global repair profile of human alkyladenine DNA glycosylase on nucleosomes reveals DNA packaging effects. *ACS Chem. Biol. 14* (8), 1687-1692.
32. Li, C.; Delaney, S. (2019) Histone H2A variants enhance the initiation of base excision repair in nucleosomes. *ACS Chem. Biol. 14* (5), 1041-1050.
33. Bilotti, K.; Tarantino, M. E.; Delaney, S. (2018) Human oxoguanine glycosylase 1 removes solution accessible 8-oxo-7,8-dihydroguanine lesions from globally substituted nucleosomes except in the dyad region. *Biochemistry 57* (9), 1436-1439.
34. Luger, K.; Rechsteiner, T. J.; Richmond, T. J. (1999) Expression and purification of recombinant histones and nucleosome reconstitution. *Methods Mol. Biol. 119*, 1-16.
35. Luger, K.; Rechsteiner, T. J.; Richmond, T. J. (1999) Preparation of nucleosome core particle from recombinant histones. *Methods Enzymol. 304*, 3-19.
36. Hayes, J. J.; Tullius, T. D.; Wolffe, A. P. (1990) The structure of DNA in a nucleosome. *Proc. Natl. Acad. Sci. U.S.A 87* (19), 7405-7409.
37. Jain, S. S.; Tullius, T. D. (2008) Footprinting protein–DNA complexes using the hydroxyl radical. *Nat. Protoc. 3* (6), 1092-1100.

38. Das, R.; Laederach, A.; Pearlman, S. M.; Herschlag, D.; Altman, R. B. (2005) SAFA: semi-automated footprinting analysis software for high-throughput quantification of nucleic acid footprinting experiments. *RNA 11* (3), 344-54.
39. Chen, F.; Tang, Q.; Bian, K.; Humulock, Z. T.; Yang, X.; Jost, M.; Drennan, C. L.; Essigmann, J. M.; Li, D. (2016) Adaptive response enzyme AlkB preferentially repairs 1-methylguanine and 3-methylthymine adducts in double-stranded DNA. *Chem. Res.Toxicol. 29* (4), 687-693.
40. Chen, F.; Bian, K.; Tang, Q.; Fedeles, B. I.; Singh, V.; Humulock, Z. T.; Essigmann, J. M.; Li, D. (2017) Oncometabolites d- and l-2-hydroxyglutarate inhibit the AlkB family DNA repair enzymes under physiological conditions. *Chem. Res. Toxicol. 30* (4), 1102-1110.
41. Vasudevan, D.; Chua, E. Y. D.; Davey, C. A. (2010) Crystal structures of nucleosome core particles containing the '601' strong positioning sequence. *J. Mol. Biol. 403* (1), 1-10.
42. Samson, L.; Derfler, B.; Boosalis, M.; Call, K. (1991) Cloning and characterization of a 3-methyladenine DNA glycosylase cDNA from human cells whose gene maps to chromosome 16. *Proc. Natl. Acad. Sci. U.S.A 88* (20), 9127-9131.
43. Chakravarti, D.; Ibeanu, G. C.; Tano, K.; Mitra, S. (1991) Cloning and expression in Escherichia coli of a human cDNA encoding the DNA repair protein N-methylpurine-DNA glycosylase. *J. Biol. Chem. 266* (24), 15710-15715.
44. Riazuddin, S.; Lindahl, T. (1978) Properties of 3-methyladenine-DNA glycosylase from Escherichia coli. *Biochemistry 17* (11), 2110-2118.
45. Olmon, E. D.; Delaney, S. (2017) Differential ability of five DNA glycosylases to recognize and repair damage on nucleosomal DNA. *ACS Chem. Biol. 12* (3), 692-701.
46. Tarantino, M. E.; Dow, B. J.; Drohat, A. C.; Delaney, S. (2018) Nucleosomes and the three glycosylases: High, medium, and low levels of excision by the uracil DNA glycosylase superfamily. *DNA Repair 72*, 56-63.
47. Beard, B. C.; Wilson, S. H.; Smerdon, M. J. (2003) Suppressed catalytic activity of base excision repair enzymes on rotationally positioned uracil in nucleosomes. *Proc. Natl. Acad. Sci. U.S.A 100* (13), 7465-70.
48. Cole, H. A.; Tabor-Godwin, J. M.; Hayes, J. J. (2010) Uracil DNA glycosylase activity on nucleosomal DNA depends on rotational orientation of targets. *J. Biol. Chem. 285* (4), 2876-85.
49. Hinz, J. M.; Rodriguez, Y.; Smerdon, M. J. (2010) Rotational dynamics of DNA on the nucleosome surface markedly impact accessibility to a DNA repair enzyme. *Proc. Natl. Acad. Sci. U.S.A 107* (10), 4646-4651.
50. Prasad, A.; Wallace, S. S.; Pederson, D. S. (2007) Initiation of base excision repair of oxidative lesions in nucleosomes by the human, bifunctional DNA glycosylase NTH1. *Mol. Cell Biol. 27* (24), 8442-8453.
51. Cai, Y.; Fu, I.; Geacintov, N. E.; Zhang, Y.; Broyde, S. (2018) Synergistic effects of H3 and H4 nucleosome tails on structure and dynamics of a lesion-containing DNA: Binding of a displaced lesion partner base to the H3 tail for GG-NER recognition. *DNA Repair 65*, 73-78.
52. Fu, I.; Cai, Y.; Zhang, Y.; Geacintov, N. E.; Broyde, S. (2016) Entrapment of a histone tail by a DNA lesion in a nucleosome suggests the lesion impacts epigenetic marking: a molecular dynamics study. *Biochemistry 55* (2), 239-242.
53. Ngo, Thuy T. M.; Zhang, Q.; Zhou, R.; Yodh, Jaya G.; Ha, T. (2015) Asymmetric unwrapping of nucleosomes under tension directed by DNA local flexibility. *Cell 160* (6), 1135-1144.

54. Lee, J.; Lee, T.-H. (2017) Single-molecule investigations on histone H2A-H2B dynamics in the nucleosome. *Biochemistry 56* (7), 977-985.
55. Odell, I. D.; Newick, K.; Heintz, N. H.; Wallace, S. S.; Pederson, D. S. (2010) Non-specific DNA binding interferes with the efficient excision of oxidative lesions from chromatin by the human DNA glycosylase, NEIL1. *DNA Repair 9* (2), 134-143.
56. Maher, R. L.; Prasad, A.; Rizvanova, O.; Wallace, S. S.; Pederson, D. S. (2013) Contribution of DNA unwrapping from histone octamers to the repair of oxidatively damaged DNA in nucleosomes. *DNA Repair 12* (11), 964-971.
57. Mao, P.; Brown, A. J.; Malc, E. P.; Mieczkowski, P. A.; Smerdon, M. J.; Roberts, S. A.; Wyrick, J. J. (2017) Genome-wide maps of alkylation damage, repair, and mutagenesis in yeast reveal mechanisms of mutational heterogeneity. *Genome Res. 27* (10), 1674-1684.
58. Pich, O.; Muinos, F.; Sabarinathan, R.; Reyes-Salazar, I.; Gonzalez-Perez, A.; Lopez-Bigas, N. (2018) Somatic and germline mutation periodicity follow the orientation of the DNA minor groove around nucleosomes. *Cell 175* (4), 1074-1087.e18.
59. Fu, I.; Cai, Y.; Geacintov, N. E.; Zhang, Y.; Broyde, S. (2017) Nucleosome histone tail conformation and dynamics: impacts of lysine acetylation and a nearby minor groove benzo[a]pyrene-derived lesion. *Biochemistry 56* (14), 1963-1973.
60. Gansen, A.; Tóth, K.; Schwarz, N.; Langowski, J. (2015) Opposing roles of H3- and H4-acetylation in the regulation of nucleosome structure—a FRET study. *Nucleic Acids Res. 43* (3), 1433-1443.
61. van Attikum, H.; Gasser, S. M. (2009) Crosstalk between histone modifications during the DNA damage response. *Trends Cell Biol. 19* (5), 207-217.
62. Montaldo, N. P.; Bordin, D. L.; Brambilla, A.; Rösinger, M.; Fordyce Martin, S. L.; Bjørås, K. Ø.; Bradamante, S.; Aas, P. A.; Furrer, A.; Olsen, L. C.; Kunath, N.; Otterlei, M.; Sætrom, P.; Bjørås, M.; Samson, L. D.; van Loon, B. (2019) Alkyladenine DNA glycosylase associates with transcription elongation to coordinate DNA repair with gene expression. *Nat. Commun. 10* (1), 5460.
63. Rinne, M.; Caldwell, D.; Kelley, M. R. (2004) Transient adenoviral *N*-methylpurine DNA glycosylase overexpression imparts chemotherapeutic sensitivity to human breast cancer cells. *Mol. Cancer Ther. 3* (8), 955-967.
64. Pilžys, T.; Marcinkowski, M.; Kukwa, W.; Garbicz, D.; Dylewska, M.; Ferenc, K.; Mieczkowski, A.; Kukwa, A.; Migacz, E.; Wołosz, D.; Mielecki, D.; Klungland, A.; Piwowarski, J.; Poznański, J.; Grzesiuk, E. (2019) ALKBH overexpression in head and neck cancer: potential target for novel anticancer therapy. *Sci. Rep. 9* (1), 13249.